International Journal of Power Electronics and Drive System (IJPEDS)
Vol. 17, No. 2, June 2026, pp. 1084~1095
ISSN: 2088-8694, DOI: 10.11591/ijpeds.v17.i2.pp1084-1095

High-efficiency two-stage LED driver with integrated PFC and LLC resonant converter for public lighting

Marref Mohammed Amine[1,2], Seyf Eddine Bechekir[2], Mokhtaria Jbilou[2], Mostefa Brahami[2], Abdelber Bendaoud[3]

[1]Institute of Applied Sciences and Technology (ISTA), University of Science and Technology of Oran Mohamed-Boudiaf (USTOMB), Oran, Algeria
[2]Intelligent Control and Electrical Power Systems (ICEPS) Laboratory, Department of Electrical Engineering, Djillali Liabès University, Sidi Bel Abbès, Algeria
[3]APELEC Laboratory, University Djillali Liabes, Sidi Bel-Abbes, Algeria

Article Info

Article history:

Received Aug 12, 2025
Revised Jan 13, 2026
Accepted Feb 21, 2026

Keywords:

LED driver
LLC resonant converter
Power factor correction
Public lighting
Total harmonic distortion
Zero-voltage switching

ABSTRACT

This paper presents the design, implementation, and experimental validation of a 150 W two-stage light-emitting diode (LED) driver integrating a power factor correction (PFC) stage and a half-bridge LLC resonant converter for public lighting applications. The problem addressed is the insufficient power quality, limited efficiency, and poor harmonic performance of conventional LED drivers used in street lighting. The proposed method combines an advanced PFC front-end with an LLC resonant converter optimized using first harmonic approximation (FHA) to achieve high efficiency, stable output regulation, and soft-switching operation. Experimental results demonstrate a significant improvement in power quality, with the input current total harmonic distortion (THD) reduced from 134% to 17%, a near-unity power factor, a regulated LED output of 31.6 V/4.72 A, and a conversion efficiency exceeding 95%. The significance of this work lies in providing a high-performance, standards-compliant driver that supports reliable, energy-efficient, and grid-friendly public lighting with reduced operational costs.

Corresponding Author:

Marref Mohammed Amine
Institute of Applied Sciences and Technology (ISTA)
University of Science and Technology of Oran Mohamed-Boudiaf (USTOMB)
B.P.1505, Oran 31000, Algeria
Email: mohammedamine.marref@univ-usto.dz

1. INTRODUCTION

Light-emitting diode (LED)-based street lighting has become the predominant choice in modern urban infrastructures due to its high energy efficiency, long lifetime, rapid switching capability, and compact design flexibility [1]–[5]. These advantages make LEDs especially suitable for large-scale public lighting systems, where reliability, energy savings, and low maintenance costs are essential [6]-[11]. To fully exploit these benefits, the associated LED driver must deliver stable and well-regulated power while maintaining high energy efficiency and compliance with international power quality standards. Despite significant progress in power electronics, many existing LED drivers still suffer from limitations such as insufficient power factor correction, elevated total harmonic distortion (THD), and reduced efficiency under varying load conditions [12], [13]. Switch-mode power supplies remain the preferred solution for LED applications due to their balance of efficiency and compactness, but they require careful design and optimization to ensure long-term reliability, controlled energy consumption, and high-quality illumination [14], [15].

Although numerous studies focus separately on improving power factor correction (PFC) circuits or refining resonant topologies, few works integrate an advanced PFC stage with a half-bridge LLC resonant converter specifically tailored to public lighting and validated through experimental prototypes [16]. This combined approach is rarely addressed in the literature, particularly when considering real operating conditions and compliance with harmonic and electromagnetic standards such as IEC 61000-3-2 and EN 55015 [17], [18]. To address these gaps, this paper introduces a 150 W two-stage LED driver that combines a high-performance PFC front-end with an optimized LLC resonant converter designed for soft switching, low harmonic distortion, and high efficiency. The design methodology includes analytical modeling of the resonant tank using the first harmonic approximation (FHA) and a detailed component sizing strategy [19]-[25]. Experimental evaluation of the developed prototype demonstrates stable LED current regulation, an efficiency exceeding 95%, and a reduction of input current THD from 134% to 17%. These results highlight the potential of the proposed architecture to meet international standards while supporting reliable, energy-efficient, and sustainable public lighting infrastructures [26].

2. METHOD

2.1. Project specifications

For this application, the main design objectives for the power converter are low cost, high-energy efficiency, and a wide operating range. The proposed 150 W LED driver adopts a two-stage architecture with five levels of power conversion, enabling an efficient distribution of functional blocks. The first stage is responsible for generating a regulated DC voltage while providing PFC. The second stage is based on an LLC resonant converter, powered by a half-bridge inverter, which efficiently drives the LED load.

Unlike conventional PWM DC-DC converters, which are generally characterized by limited efficiency due to the lack of galvanic isolation and precise current control, the half-bridge LLC topology offers superior LED current regulation and significantly higher efficiency. Moreover, this approach helps reduce the cost and size of the LED driver system. Compared to the LCC topology, the LLC topology provides better energy efficiency thanks to its lower switching losses and its ability to operate in resonant mode over a wider load range. While the LCC topology can achieve stricter voltage regulation, it often results in higher control complexity and greater losses at light load. Therefore, the LLC topology represents an optimal compromise between performance, efficiency, and implementation simplicity, making it particularly well-suited for high-efficiency LED driver applications. The LED driver we propose is based on a two-stage architecture, comprising a resonant LLC converter and a PFC stage, as illustrated in Figure 1.

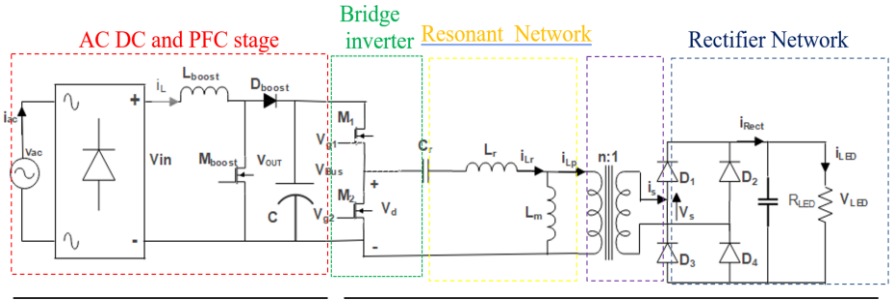

Figure 1. The proposed LED driver is based on an LLC resonant converter

2.2. Justification for selecting the half-bridge LLC topology

The converter selected for output current regulation is based on the LLC resonant topology, as illustrated in Figure 2. It consists of two power switches (M1 and M2), a series capacitor (C_r), a series inductor (L_r), a parallel inductor (L_m), an optional transformer, a full-bridge rectification stage (D1, D2, D3, D4), and an output filter capacitor (C_0).

The main advantage of the LLC resonant topology lies in its ability to achieve zero-voltage switching (ZVS) for the switching devices M1 and M2 over the entire operating range. Unlike the series resonant converter, the LLC converter can operate efficiently under light-load conditions by increasing the switching frequency. In this case, the impedance of the parallel inductor L_m increases proportionally with frequency, which prevents an increase in circulating current under light loads a common drawback in conventional parallel resonant topologies.

As previously mentioned, the LLC resonant topology combines the benefits of both series and parallel resonant circuits while eliminating their respective limitations. It supports a wide load range, while

maintaining a limited switching frequency variation and minimizing circulating current within the resonant tank. Moreover, the LLC converter provides multiple degrees of design flexibility, making it highly adaptable to specific application requirements. Its design is further simplified by the use of the FHA method, which facilitates accurate modeling and optimization.

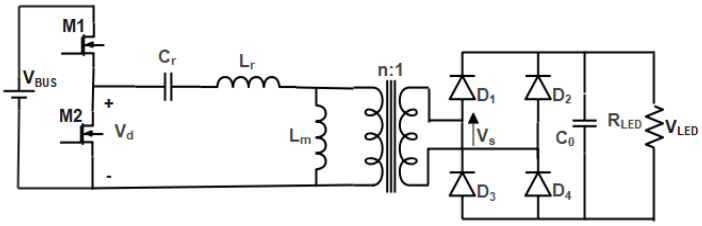

Figure 2. Second stage of the proposed LLC-Type LED driver

2.3. Operating principle of the LLC resonant topology

The analysis of the LLC resonant converter is significantly simplified by applying the FHA of the square waveforms. The LLC resonant tank acts as a filter, attenuating the higher-order harmonics of the square-wave voltage supplied by the inverter. As a result, the output power is primarily transferred through the fundamental frequency component of the waveform. This approximation is applied directly to the input voltage, which is a square wave generated by switches M1 and M2 from a DC source. The square waveform is then approximated as a sinusoidal waveform at the same fundamental frequency for the purpose of analysis and design.

2.4. Input voltage characteristics

The input voltage to the LLC converter, denoted as *VBus*, is the regulated DC voltage provided by the first stage. The switches M1 and M2 operate at a 50% duty cycle, with a 180° phase shift between them, producing a square-wave voltage oscillating between 0 V and *VBus*. The DC component, equal to *VBus* /2, is blocked by the series capacitor *Cr*, resulting in an AC waveform centered at 0 V, swinging between –*VBus* /2 and + *VBus* /2, as illustrated in Figure 3. The corresponding sinusoidal voltage at the output of the resonant tank, derived under the First Harmonic Approximation, is denoted as Vd_{FHA}, and is also shown in Figure 3.

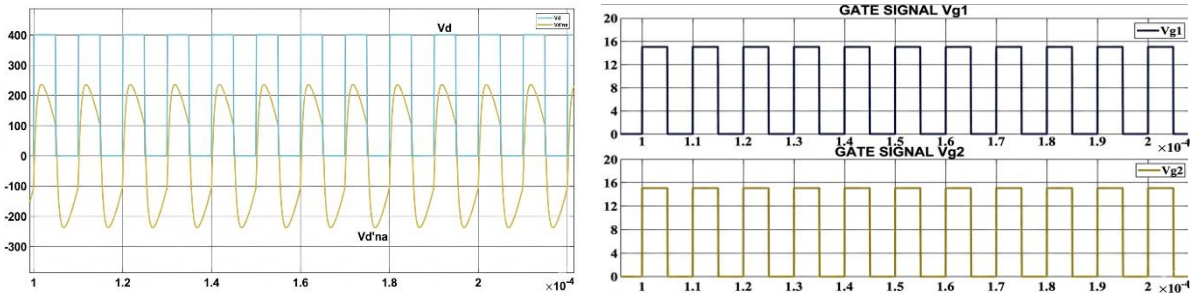

(a) (b)

Figure 3. Simulation results for the system: (a) output voltage waveform generated by switches M1 and M2 and (b) simulated gate-drive signal

The harmonics of the voltage at the output of the half-bridge inverter are filtered by the resonant tank composed of C_r, L_r, and L_m. As a result, the current becomes sinusoidal, and the power delivered to the converter's output is mainly derived from the fundamental frequency component. The input voltage is therefore expressed using the first harmonic approximation, as shown in (1).

$$Vd_{FHA} = (4.V_{Bus} / 2.\pi) \sin(wt) \quad (1)$$

2.5. Equivalent resistance

Figure 4 shows a simplified schematic of a half-bridge LLC resonant converter, where L_m. is the magnetizing inductance, L_r is the series resonant inductance, and C_r is the resonant capacitor. It also presents the

typical waveforms of the LLC resonant converter. The operating frequency is assumed to match the resonant frequency, determined by the resonance between L_r and C_r. Since the magnetizing inductance is relatively low, a significant magnetizing current L_m flows freely on the primary side without contributing to power transfer. The primary current Ip is the sum of the magnetizing current and the reflected secondary current.

In general, the second stage of the LLC resonant topology consists of three main parts, as illustrated in Figure 4: a square-wave generator, a resonant tank circuit, and a fast-output rectification stage. The resonant circuit consists of a capacitor, leakage inductances, and the magnetizing inductance of the transformer. It acts as a filter for high-order harmonic currents. In practice, only a sinusoidal current can flow through the resonant tank, even when a square-wave voltage is applied to it. The primary current Ip lags behind the voltage applied to the resonant circuit, namely, the fundamental component of the square-wave voltage Vd generated by the half-bridge totem enabling ZVS of the MOSFETs. The rectifier stage generates a DC output voltage by rectifying the AC current using diodes and a filter capacitor C0. The rectifier can be implemented either as a full-bridge configuration or a center-tap structure with capacitive output filtering.

Thanks to the filtering action of the resonant circuit, the fundamental approximation can be used to determine the voltage gain of the resonant converter. This approximation assumes that only the fundamental component of the input square wave contributes to power transfer toward the output. Since the secondary-side rectifier acts as an impedance transformer, the equivalent load resistance differs from the actual load resistance. Figure 5 illustrates the model of this equivalent load resistance. The primary circuit is represented by a sinusoidal current source i_{sFHA}, and a square-wave voltage Vs appears at the rectifier input. The output current i_{sFHA} is then determined as (2):

$$Is_{FHA} = (I_{LED} * \pi /2)\ sin(wt) \quad (2)$$

Vs_{FHA} is given as (3) and (4):

$$Vs_{FHA} = +V_{LED}\ if\ sin\ (wt) > 0 \quad (3)$$

$$Vs_{FHA} = -\ V_{LED}\ if\ sin(wt) < 0 \quad (4)$$

The fundamental harmonic equation of Vs_{FHA} is given as (5):

$$Vs_{FHA} = (4.V_{LED}/\pi)sin\ (wt) \quad (5)$$

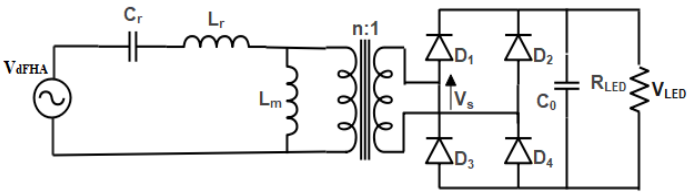

Figure 4. Simplified AC equivalent circuit of the LLC converter

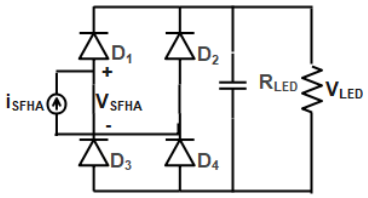

Figure 5. Derivation of the equivalent load resistance Rac

After this process, the voltage and current at the transformer primary become sinusoidal and in phase with each other. The transformer, rectifier, output filter, and load can therefore be replaced by an equivalent resistance connected in parallel with the magnetizing inductance L_m. Since the harmonic component of Vs_{FHA} does not contribute to power transfer, the equivalent AC load resistance on the secondary side can be calculated by dividing Vs_{FHA} by by Is_{FHA}, as shown in (6), and the equivalent circuit model is illustrated in Figure 6.

$$Rac_s = Vs_{FHA}/\ Is_{FHA} = 8.V_{LED}/\ \pi^2.\ I_{LED},\ Rac_s = \frac{8}{\pi^2}.R_{LED} \quad (6)$$

We now proceed to the next step, which consists of transferring the resistance R_{acs} from the secondary side to the primary side. This can be achieved using the transformer turns ratio and the resistance transformation equation. Given the turns ratio ($n = \frac{Np}{Ns}$), the equivalent load resistance R_{acs} referred to the primary side is obtained as (7).

$$Rac_p = \frac{8.n^2}{\pi^2} * R_{LED} \quad (7)$$

After applying the necessary steps for the first harmonic approximation, the circuit in the referenced figure can be analyzed in its simplified form, as illustrated in Figure 7.

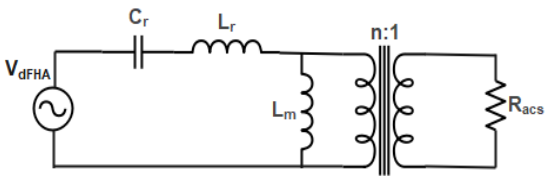

Figure 6. R_{acs} Approximation of the output circuit

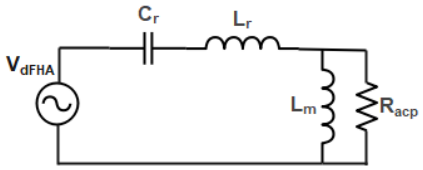

Figure 7. Simplified output circuit of the converter

2.6. Transfer function of the LLC-led driver

The LLC resonant circuit, simplified using the first harmonic approximation of the square-wave signals, is illustrated in Figure 8. This approximation allows the complex switching waveforms to be represented by their fundamental sinusoidal component, which simplifies the analysis of the resonant behavior. The model provides an effective way to study the voltage and current characteristics of the converter under steady-state operation. Therefore, it is widely used in the design and optimization of high-efficiency LLC resonant converters.

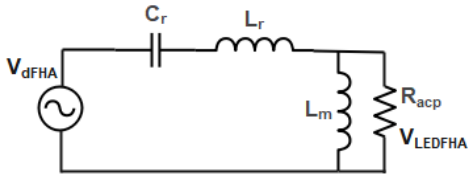

Figure 8. AC equivalent circuit of the proposed LED driver

The equivalent electrical circuit is a voltage divider: the voltage ratio is equal to the ratio of the impedances.

$$M(p) = \frac{VLEDFHA(p)}{VdFHA(p)} = \frac{Zp}{Zs+Zp} \tag{8}$$

$$\begin{cases} Zs(p) = Lr * P + \frac{1}{Cr*P} \\ \frac{1}{Zp} = \frac{1}{Racp} + \frac{1}{Lm*P} \end{cases} \rightarrow \begin{cases} Zs(p) = Lr * P + \frac{1}{Cr*P} \ , P = jw \\ Zp(p) = \frac{Lm*P}{1+(\frac{Lm}{Racp})*P} \end{cases} \tag{9}$$

$$M(j\omega) = \frac{VLEDFHA}{VdFHA} = \frac{(\mathrm{m}-1)\left(\frac{\omega}{\omega 0}\right)^2}{\left(\frac{\omega^2}{\omega p^2}-1\right)+\left(\frac{\mathrm{Q}(\mathrm{m}-1)}{\omega 0}\right)\left(\frac{\omega^2}{\omega 0^2}-1\right)*j\omega} \tag{10}$$

$$M_v = \frac{VLEDFHA}{VdFHA} = \frac{VsFHA*n}{VdFHA} = \frac{\frac{4n.Vled}{\pi}\sin(\omega t)}{\frac{4\,VBus}{2\,\pi}\sin(\omega t)} = \frac{2n\,.Vled}{VBus} \tag{11}$$

Or:

$$Q = \frac{1}{Rac_p}\sqrt{\frac{Lr}{Cr}},\ \omega_p = \frac{1}{\sqrt{Lp.Cr}},\ \omega_0 = \frac{1}{\sqrt{Lr.Cr}},\ Rac_p = \frac{8.n^2}{\pi^2} * R_{LED} \tag{12}$$

$$L_p = L_r + L_m,\ m = \frac{Lp}{Lr},\ Mv = \sqrt{\frac{m}{m-1}}\ a\ \omega_0 = \omega \tag{13}$$

As shown in (10), there are two resonance frequencies: one determined by L_r and C_r, and the other determined by L_p and Cr. In (14) indicates that the voltage gain is equal to unity at the resonance frequency (ω_0), regardless of load variations, and is given by (14).

$$M_v = \frac{(m-1).\omega_p{}^2}{\omega_0{}^2 - \omega_p{}^2} = \frac{2n\,.Vled}{VBus} = 1\ a\omega = \omega_0 \quad (14)$$

2.7. LED selection

For this work, 5730-type LEDs were selected, each rated at 0.5 W, operating at a forward voltage between 3 V and 3.4 V with a nominal current of 150 mA. To form a 50 W module, two strings of ten LEDs connected in series were assembled in parallel. Three of these 50 W modules were then connected in parallel, achieving a total power of 150 W. The supply voltage of the system is between 30 V and 34 V (V_{LED}).

2.8. Calculation of resonant circuit parameters

According to the relation: $P_{Led} = V_{Led} * I_{Led}$ *:*

$$I_{Led} = 4.69A \quad (15)$$

We also have: $P_{Led} = R_{Led} * i_{Led}^2$. Thus, the LED resistance is calculated as (16).

$$R_{led} = 6.82\Omega \quad (16)$$

For the input voltage amplitude V_{dFHA}, we take the value of the fundamental harmonic:

$$V_{dFHA} = \frac{4*(Vbus/2)}{\pi} = 254.6\ V \text{ with } V_{Bus} = 400\ V \quad (17)$$

For the LED voltage amplitude V_{LEDFHA}, we also take the value of the fundamental harmonic:

$$V_{LEDFHA} = \frac{4*VLED}{\pi} = 41\ V \quad (18)$$

The filter gain is calculated by (19).

$$Mv = \sqrt{\frac{m}{m-1}} = 1.12,\ m = 5 \quad (19)$$

Transformer turns ratio selection:

$$n = \frac{Np}{Ns} = \frac{VBus}{2*VLED} * M_v \quad (20)$$
$$n = 7$$

The equivalent LED resistance in the simplified model R_{acp} is determined by (21).

$$R_{acp} = \frac{8\,.n^2}{\pi^2} * R_{LED} = 270,88\ \Omega \quad (21)$$

The quality factor is set to: $Q = 0.4 < 1$. Therefore, for the series resonant circuit parameters, imposing Q and $\omega_0 = 2\pi * f_0$, we have:

$$Z_r = Lr * \omega_0 = \frac{1}{Cr*\omega 0} \Longrightarrow Z_r = R_{acp} * Q,\ Zr = \sqrt{\frac{Lr}{Cr}} \quad (22)$$

$$L_r = \frac{Racp*Q}{\omega 0} \text{ and } C_r = \frac{1}{Q*\omega 0*Racp} \quad (23)$$

Finally, the magnetizing inductance L_p is defined by the inductance ratio: $m = L_P / L_r = 5$. ($L_P = L_m + L_r$) A sufficient value of m ensures current stability through the LEDs. The parallel resonant frequency is given by:

$$\omega_p = \frac{1}{\sqrt{(Lr + Lm).Cr}} \quad (24)$$

2.9. Calculated parameters

Finally, based on the design of the resonant circuit, the calculated passive component values are summarized in Table 1. These parameters are derived from the proposed design methodology, considering the required operating conditions of the LLC resonant converter. The selection of these components ensures optimal resonant behavior, improved efficiency, and stable operation under varying load conditions.

Table 1. Calculated parameters of the proposed LED driver

Parameters	Desing	Parameters	Desing
L_m	688 µH	m	5
L_r	172 µH	Q	0.4
C_r	14.68 nF	M_v	1.12
f_0	100 KHZ	n	7

2.10. Bode diagram

The Bode diagram of the system is shown in Figure 9. It highlights the frequency response of the proposed filter, clearly illustrating the lower and upper cutoff frequencies as well as the corresponding bandwidth. This analysis makes it possible to assess the system's stability and dynamic behavior, confirming the effectiveness of the filter within the intended operating range.

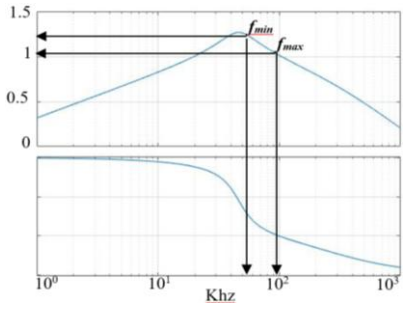

Figure 9. Bode diagram of the system

2.11. Determination of maximum and minimum voltage gains

The maximum and minimum voltage gains are calculated as (25) and (26):

$$M_{min} = \frac{2.VLED}{VBusmax} * n = \frac{2.32}{410} * 7 = 1.09 \quad (25)$$

$$M_{max} = \frac{2.VLED}{VBusmin} * n = \frac{2.32}{390} * 7 = 1.14 \quad (26)$$

To prevent the operating point from entering the capacitive region, the maximum voltage gain must include a design margin. This margin is set to 0.15 × M_{max}. Therefore, the value of M_{max} is adjusted as (27):

$$M_{max} = 1.14 * 1.15 = 1.31 \quad (27)$$

2.12. Determination of the switching frequency range

The minimum switching frequency f_{min} and the maximum switching frequency f_{max} are calculated and presented:

$$f_{max} = \frac{1}{2.\pi\sqrt{Lr.Cr}} = 99\ KHz \quad (28)$$

$$f_{min} = \frac{fr}{\sqrt{1+K(1-\frac{1}{Mmax^2})}} = 61.7\ KHz,\ k = \frac{Lm}{Lr} \quad (29)$$

3. IMPLEMENTATION

Figure 10 presents the overall functional block diagram of the developed system. It includes a control board designed to drive the half-bridge inverter as well as the measurement devices. The LED driver integrates both the half-bridge inverter and the LLC resonant circuit, supplied by a DC bus voltage (V_{BUS}) generated from a PFC stage. The complete system drives a 150 W 5730-type LED lamp.

Although the integrated transformer approach in LLC resonant converter design allows combining the magnetic components L_r and L_m into a single core thus reducing the magnetic component count—the value of L_r is difficult to control in the practical design of a transformer. Designing the resonant circuit sometimes requires iterative adjustments to account for the final L_r value obtained after transformer construction. The final design of the resonant network is summarized in Table 1.

3.1. Final resonant network design

To evaluate the efficiency of the proposed LED driver, a prototype was built and tested. Table 2 summarizes the system specifications of the proposed converter along with the characteristics of the components employed. The design process considered several key parameters, including LED selection, transformer turns ratio (n), maximum (M_{max}) and minimum (M_{min}) voltage gain, effective resistive load reflected to the transformer primary (R_{acp}), inductance ratio (m) between magnetizing and resonant inductances, quality factor (Q), resonant frequency (f_r), and the values of the series resonant capacitor (C_r), resonant inductance (L_r), and magnetizing inductance (L_m).

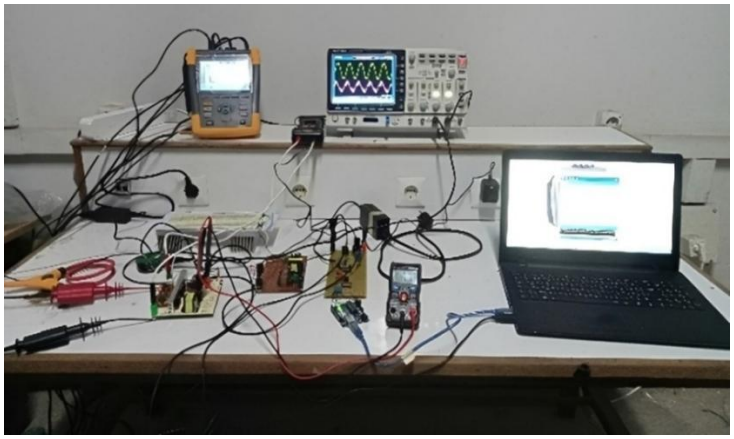

Figure 10. Photo of the proposed prototype

Table 2. Practical specifications of the proposed LED driver

Parameters	Final design	Parameters	Final design
L_p	580 µH	m	4.9
L_r	118 µH	Q	0.4
C_r	15 nF/1000V	M_v	1.12
f_0	98 KHZ	n	7

3.2. Experimental result

Experimental tests were performed on the developed LLC-based LED driver to validate the theoretical calculations and simulation results. The prototype integrates a half-bridge inverter stage along with a PFC front-end. As an initial step, gate drive signals were tested to ensure proper operation. Figure 11 shows the measured gate voltages applied to the MOSFETs at a switching frequency of 98 kHz, confirming compliance with the design specifications. Figure 12 depicts the measured waveforms of V_d and V_{dFHA}, whereas Figure 13 shows V_s and I_s. Under nominal load conditions, Figure 14 illustrates the resonant capacitor voltage (V_{cr}), the resonant inductor current (i_{Lr}), and the voltage V_d within the LLC resonant tank. Finally, Figure 15 presents the measured voltage and current across a 150 W LED lamp in steady-state operation, demonstrating stable performance and high-quality power delivery from the driver.

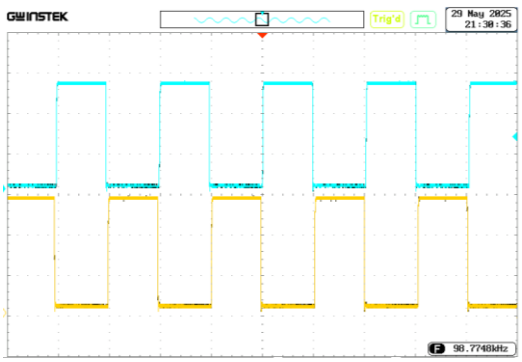

Figure 11. Waveforms at rated load V_{g1} ;V_{g2}

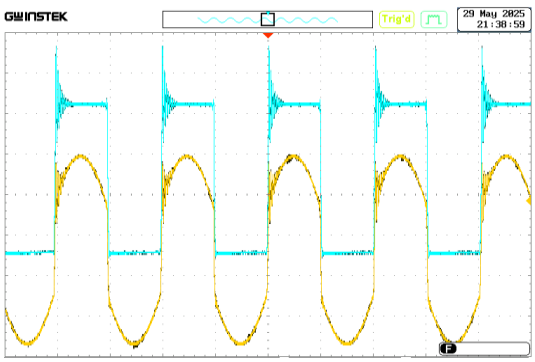

Figure 12. Waveforms at rated load V_d ;V_{dFHA}

3.3. Study of total harmonic distortion and power factor correction of the input current and improved results discussion

The analysis shows that the proposed system with a PFC stage reduces the THD of the input current from over 134% (Figure 16) to around 17% (Figure 17). This significant reduction demonstrates improved power quality and compliance with electrical grid harmonic standards. In terms of efficiency, the developed prototype achieves a measured conversion efficiency exceeding 95%. This performance is comparable to or superior to several reported LED driver architectures. For example, the CrCM boost PFC combined with an LLC resonant converter in [6] reaches efficiencies around 92–94%, while the single-stage soft-switching driver in [7] achieves approximately 90%. Similarly, the high-brightness LED driver presented in [12] reports efficiencies near 94%. The proposed design, therefore, offers improved efficiency while simultaneously reducing THD more effectively than many existing solutions.

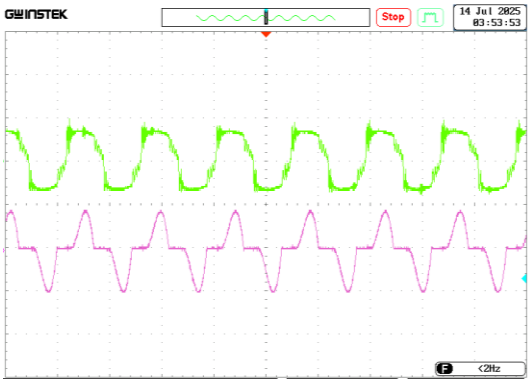

Figure 13. Waveforms at rated load V_s ; Is

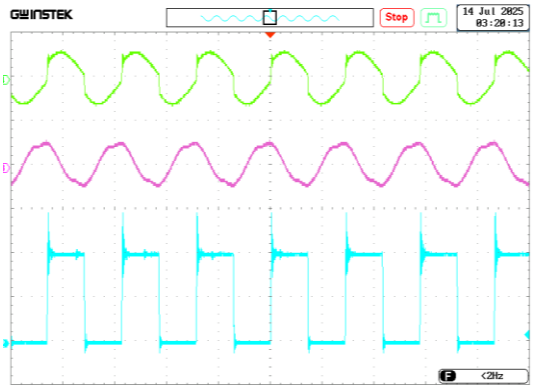

Figure 14. Waveforms at rated load V_{cr} ; i_{Lr} ; V_d

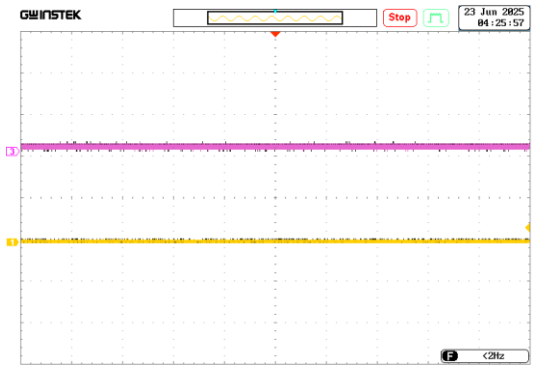

Figure 15. Obtained the current–voltage result of the LEDs

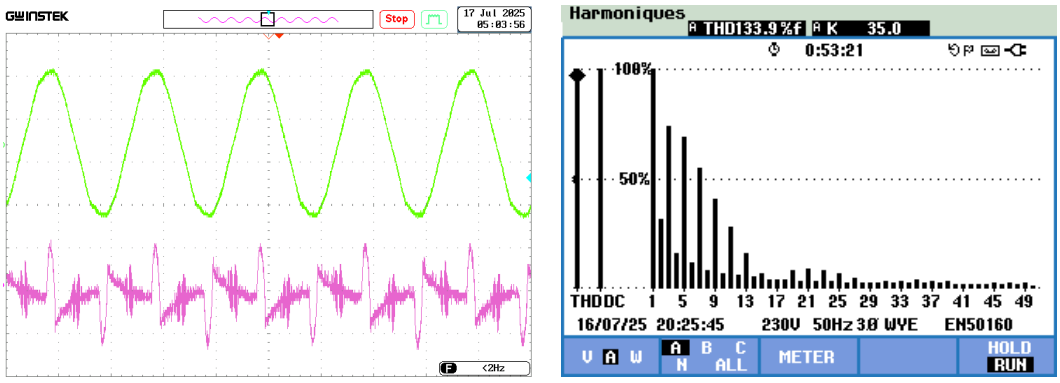

Figure 16. Voltage and current and THD analysis of current AC without PFC

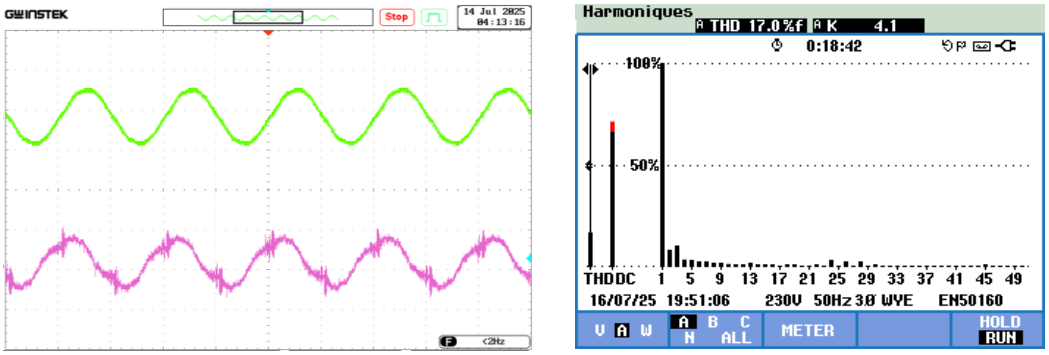

Figure 17. Voltage and current and THD analysis of current AC with PFC

4. CONCLUSION

This study designed and experimentally validated a 150 W two-stage LED driver integrating a high-performance PFC stage and a half-bridge LLC resonant converter for public lighting applications. The proposed architecture effectively addresses the limitations identified in conventional LED drivers by providing stable output regulation, soft-switching operation, and improved compatibility with grid power quality requirements. The experimental results demonstrate significant performance improvements. The input current THD was reduced from more than 134% to approximately 17%, the power factor reached values close to 0.99, and the overall efficiency exceeded 95%. These results confirm the effectiveness of combining an advanced PFC front-end with an optimized LLC resonant stage to achieve high efficiency and grid-compliant operation in outdoor lighting systems.

Despite its strong performance, the system presents certain limitations. The practical design of the transformer, particularly the precise tuning of the resonant inductances, requires iterative adjustments. Moreover, thermal management becomes increasingly important at higher power levels or in enclosed lighting fixtures. Future work may explore the use of adaptive or digital control techniques, integration with smart grid infrastructures and communication-based lighting networks, as well as scaling the proposed design to higher-power LED systems suitable for next-generation urban lighting applications.

FUNDING INFORMATION

This research received no external funding.

AUTHOR CONTRIBUTIONS STATEMENT

This journal uses the Contributor Roles Taxonomy (CRediT) to recognize individual author contributions, reduce authorship disputes, and facilitate collaboration.

Name of Author	C	M	So	Va	Fo	I	R	D	O	E	Vi	Su	P	Fu
Marref Mohammed Amine	✓	✓	✓	✓	✓	✓		✓	✓	✓		✓	✓	
Seyf Eddine Bechekir		✓		✓		✓		✓	✓	✓	✓	✓		
Mokhtaria Jbilou	✓		✓	✓			✓			✓	✓		✓	✓
Mostefa Brahami		✓	✓		✓		✓		✓			✓		✓
Abdelber Bendaoud			✓		✓		✓			✓		✓		✓

C : **C**onceptualization
M : **M**ethodology
So : **So**ftware
Va : **Va**lidation
Fo : **Fo**rmal analysis
I : **I**nvestigation
R : **R**esources
D : **D**ata Curation
O : Writing - **O**riginal Draft
E : Writing - Review & **E**diting
Vi : **Vi**sualization
Su : **Su**pervision
P : **P**roject administration
Fu : **Fu**nding acquisition

CONFLICT OF INTEREST STATEMENT

Authors state no conflict of interest.

DATA AVAILABILITY

The data and simulation models used in this study are available from the author upon reasonable request.

REFERENCES

[1] T. Tayar, A. Abramovitz, and D. Shmilovitz, "DCM boost PFC for high brightness LED driver applications," *Energies*, vol. 14, no. 17, p. 5486, Sep. 2021, doi: 10.3390/en14175486.

[2] M. S. Zaky, H. Z. Azazi, and E. Touti, "PFC control for LED lamp driver using sensorless predictive current controller," *Engineering, Technology & Applied Science Research*, vol. 8, no. 5, pp. 3373–3379, Oct. 2018, doi: 10.48084/etasr.2283.

[3] F. Ferdous, M. Hassan, N. Rahman, T. Hassan, and R. Islam, "Design of an energy efficient buck based LED driver in DCM and CCM," *European Journal of Engineering and Technology Research*, vol. 9, no. 3, 2024, doi: 10.24018/ejeng.2024.9.3.3169.

[4] D. A. Gowthaman and E. K. Arulmozhi, "Enhancing power factor on LED light driver with boost and fly back converter integration," *International Journal for Research in Applied Science and Engineering Technology*, vol. 11, no. 11, pp. 1934–1940, Nov. 2023, doi: 10.22214/ijraset.2023.56996.

[5] J. Ma, Y. Sun, and L. Hu, "A single-stage bridgeless LLC resonant converter with constant frequency control based LED driver," *IET Power Electronics*, vol. 14, no. 15, pp. 2507–2518, Nov. 2021, doi: 10.1049/pel2.12198.

[6] S. Pal, B. Singh, and A. Shrivastava, "Quasi-constant bus voltage CrCM boost PFC fed LLC resonant converter in high power LED lighting systems," *International Journal of Circuit Theory and Applications*, vol. 49, no. 6, pp. 1583–98, 2021, doi: 10.1002/cta.2965.

[7] C.-A. Cheng, C.-H. Chang, H.-L. Cheng, E.-C. Chang, T.-Y. Chung, and M.-T. Chang, "A single-stage LED streetlight driver with soft-switching and interleaved PFC features," *Electronics*, vol. 8, no. 8, p. 911, Aug. 2019, doi: 10.3390/electronics8080911.

[8] M. Faizan, J. Bi, M. Liu, L. Wang, V. Stempitsky, and M. Z. Yousaf, "Long life power factor corrected LED driver with capacitive energy mechanism for street light applications," *Sustainability*, vol. 15, no. 5, p. 3991, Feb. 2023, doi: 10.3390/su15053991.

[9] J. Ma, X. Wei, L. Hu, and J. Zhang, "LED driver based on boost circuit and LLC converter," *IEEE Access*, vol. 6, pp. 49588–49600, 2018, doi: 10.1109/ACCESS.2018.2866502.

[10] Y. Hu and M. M. Jovanovic, "LED driver with self-adaptive drive voltage," *IEEE Transactions on Power Electronics*, vol. 23, no. 6, pp. 3116–3125, Nov. 2008, doi: 10.1109/TPEL.2008.2004558.

[11] X. Qu et al., "A novel LLC resonant converter for LED lighting applications with high efficiency," IEEE Transactions on Industrial Electronics, vol. 60, no. 9, pp. 4212–4220, 2013.

[12] E. Sehirli and Ö. Üstün, "Design and implementation of high-power factor isolated Ćuk converter-based LED driver with SiC MOSFET," *Electrical Engineering*, vol. 105, no. 1, pp. 465–476, Feb. 2023, doi: 10.1007/s00202-022-01679-1.

[13] Y. Hu et al., "A high power factor and high efficiency LED driver with integrated PFC," IEEE Transactions on Power Electronics, vol. 29, no. 9, pp. 4739–4749, 2014.

[14] D. Karunatilaka, F. Zafar, V. Kalavally, and R. Parthiban, "LED based indoor visible light communications: state of the art," *IEEE Communications Surveys & Tutorials*, vol. 17, no. 3, pp. 1649–1678, 2015, doi: 10.1109/COMST.2015.2417576.

[15] M. Nassary, M. Orabi, M. Arias, E. M. Ahmed, and E.-S. Hasaneen, "Analysis and control of electrolytic capacitor-less LED driver based on harmonic injection technique," *Energies*, vol. 11, no. 11, 2018, doi: 10.3390/en11113030.

[16] J. W. Kolar and J. Miniböck, "A review of single-phase power factor correction techniques for high-efficiency LED drivers," IEEE Transactions on Power Electronics, vol. 28, no. 4, pp. 1810–1825, 2013.

[17] L. Zhai, T. Zhang, Y. Cao, S. Yang, S. Kavuma, and H. Feng, "Conducted EMI prediction and mitigation strategy based on transfer function for a high-low voltage DC-DC converter in electric vehicle," *Energies*, vol. 11, no. 5, p. 1028, Apr. 2018, doi: 10.3390/en11051028.

[18] R. Keskin and I. Aliskan, "Design of non-inverting buck-boost converter for electronic ballast compatible with LED drivers," *arXiv*, Apr. 2019, [Online]. Available: http://arxiv.org/abs/1907.09890

[19] A. Brajdić, "LLC type galvanic isolated resonant converter," *arXiv*, May 2023, [Online]. Available: http://arxiv.org/abs/2305.18132

[20] R. Stevenson, "The LED's dark secret: Solid-state lighting won't supplant the lightbulb until it can overcome the mysterious malady known as droop," *IEEE Spectrum*, vol. 46, no. 8, pp. 30–37, 2009.

[21] P. Stumpf, A. Lorincz, and I. Nagy, "Stability of digitally controlled PFC boost converter with auxiliary state vector," in *2013 IEEE International Symposium on Industrial Electronics*, May 2013, pp. 1–6, doi: 10.1109/ISIE.2013.6563861.

[22] D. Maheswaran and S. V T, "A commercial low cost, highly efficient UC3842 based high brightness LED (HBLED) Lamp," *International Journal of Power Electronics and Drive Systems (IJPEDS)*, vol. 9, no. 1, pp. 1-7, 2018, doi: 10.11591/ijpeds.v9.i1.pp1-7.

[23] R. Haroun, A. Cid-Pastor, A. El Aroudi, and L. Martinez-Salamero, "Synthesis of canonical elements for power processing in DC distribution systems using cascaded converters and sliding-mode control," *IEEE Transactions on Power Electronics*, vol. 29, no. 3, pp. 1366–1381, Mar. 2014, doi: 10.1109/TPEL.2013.2261093.

[24] A. Ramezani, S. Farhangi, H. Iman-Eini, B. Farhangi, R. Rahimi, and G. R. Moradi, "Optimized LCC series compensated resonant network for stationary wireless EV chargers," *IEEE Transactions on Industrial Electronics*, vol. 66, no. 4, pp. 2756–2765, Apr. 2019, doi: 10.1109/TIE.2018.2840502.

[25] M. M. Amine, H. Habib, and S. E. Bechekir, "Realization of an dimmable electronic ballast for a discharge lamps fed by an LSCSCP circuit and a PFC stage," *International Journal of Power Electronics and Drive Systems (IJPEDS)*, vol. 13, no. 2, p. 643, Jun. 2022, doi: 10.11591/ijpeds.v13.i2.pp643-656.

[26] S. Martins, L. Roggia, M. S. Perdigão, and Á. R. Seidel, "Planar magnetic regulator applied to an LLC converter for CCT control," *IEEE Transactions on Power Electronics*, vol. 39, no. 10, pp. 13300–13308, Oct. 2024, doi: 10.1109/TPEL.2024.3410232.

BIOGRAPHIES OF AUTHORS

Marref Mohammed Amine was born in SidiBel-Abbès, Algeria, in 1990. He received a Ph.D. in electrical engineering from the University of SidiBel-Abbès, where he is currently a professor in the Department of Electrical Engineering at the University of Oran at the Institute of Applied Sciences (ISTA). Specializing in electrotechnics and machine control, at the Intelligent Control and Electrical Energy Systems Laboratory (ICEPS) of the Department of Electrical Engineering at Djillali Liabes University in the city of SidiBel-Abbès, Algeria. His current research focuses on power electronic converters and the optimization of public lighting. He can be contacted at email: mohammedamine.marref@univ-usto.dz.

Seyf Eddine Bechekir was born in Bouira, Algeria, in 1991. In 2021, he received his doctorate degree in electrical engineering from the University of Sidi Bel-Abbes, where he is currently a professor and tutor in the Department of Electrical Engineering. Between 2015 and 2021, he joined the Intelligent Control and Electrical Power Systems Laboratory at the University of Sidi Bel-Abbes. His current research interests include the application of power electronics converters and plasma technology. He has published numerous research papers in international journals and conference proceedings. He can be contacted at email: seyfeddine.electrotechnique@gmail.com.

Mokhtaria Jbilou was born in Sidi Bel-Abbes, Algeria, in 1971. She received the B.I., engineering degree, M.Sc., and Ph.D. degrees in electrical engineering from the University of DjilaliLiabes, SidiBel-Abbes, in 1994, 1998, 2013, and 2019, respectively. She has been an engineer and auditor in the Energy Department, where she has gained significant professional experience in the field of renewable energies since 2006. Since 2016, she has been a professor of electrical engineering at the same university. Her current research interests include the application of power electronics converters and plasma technology. She has published numerous research papers in international journals and conference proceedings. She can be contacted at email: harmel71@yahoo.fr.

Mostefa Brahami was born in Tlemcen, Algeria, in 1956. He earned his engineering degree in electrical engineering from the University of Sciences and Technology of Oran, Algeria, in 1982. From 1984 to 1992, he worked as a service manager and trainer with the national electronics industry company. Since 1992, he has been teaching at Djillali Liabes University of Sidi Bel-Abbes, where he earned his Ph.D. in 2003 under the supervision of Professor Pol Pirotte from the University of Liège, Belgium. His doctoral research focused on electric power systems and their environmental impacts. Since 2010, he has served as the director of the "Intelligent Control and Electrical Power Systems" research laboratory. He can be contacted at email: mbrahami@yahoo.com.

Abdelber Bendaoud received the Eng. degree in electrical engineering from the University of Sciences and Technology, Oran, Algeria, in 1982, the M.S. degree in 1999, and the doctorate degree in 2004 from the Electrical Engineering Institute of Sidi Bel-Abbes University, Algeria. Since 1994, he has worked as a professor at the Electrical Engineering Department, University of SidiBel Abbes, Algeria. He is also Head of the Electromagnetic Compatibility Research Group of APELEC Laboratory. He has published several scientific papers in international and national journals, as well as in conference proceedings. His current research interests: power electronics, electrostatic separation technologies, high voltage, corona discharge, LED Lighting, and electromagnetic compatibility (EMC). He can be contacted at email: babdelber@gmail.com.